UNIVERSITY OF
FORWARD
THINKING
WESTMINSTER

WestminsterResearch
http://www.westminster.ac.uk/westminsterresearch

In Vivo Tracking and 1H/19F Magnetic Resonance Imaging of Biodegradable Polyhydroxyalkanoate / Polycaprolactone Blend Scaffolds Seeded with Labeled Cardiac Stem Cells

Constantinides, C., Basnett, P., Lukasiewicz, B., Carnicer, R., Swider, E., Majid, Q.A., Srinivas, M., Carr, C.A. and Roy, I.

This document is the Accepted Manuscript version of a Published Work that appeared in final form in ACS Applied Materials and Interfaces, copyright © American Chemical Society after peer review and technical editing by the publisher.

To access the final edited and published work see:

https://dx.doi.org/10.1021/acsami.8b06096

The WestminsterResearch online digital archive at the University of Westminster aims to make the research output of the University available to a wider audience. Copyright and Moral Rights remain with the authors and/or copyright owners.

Whilst further distribution of specific materials from within this archive is forbidden, you may freely distribute the URL of WestminsterResearch: ((http://westminsterresearch.wmin.ac.uk/).

In case of abuse or copyright appearing without permission e-mail repository@westminster.ac.uk

In Vivo Tracking and $^{1}H/^{19}F$ MRI of Biodegradable Polyhydroxyalkanoate/Polycaprolactone Blend Scaffolds Seeded with Labeled Cardiac Stem Cells

Christakis Constantinides[1*], Pooja Basnett[2], Barbara Lukasiewicz[2], Ricardo Carnicer[1], Edyta Swider[3], Qasim A. Majid[4], Mangala Srinivas[3], Carolyn A. Carr[5], Ipsita Roy[2]

Correspondence Address: *Dr. C. Constantinides
Chi-Biomedical Ltd.
Nicosia
Cyprus
[1]Radcliffe Department of Medicine
Wellcome Trust Centre for Human Genetics
Department of Cardiovascular Medicine
University of Oxford
Roosevelt Drive, Old Road Campus, Headington
Oxford OX3 7BN
UK
Tel: +357 96711475/+35722345839
Email: Christakis.Constantinides@gmail.com
[2]Applied Biotechnology Research Group, Faculty of Science and Technology, University of Westminster
115 New Cavendish Street
London W1W 6UW
UK
[3]Radboud University Medical Center (Radboud UMC)
Department of Tumor Immunology, 278
Radboud Institute for Molecular Life Sciences (RIMLS)
Postbox 9101
6500HB Nijmegen
The Netherlands
[4]Department of Myocardial Function
National Heart and Lung Institute
Imperial College London
London, W12 0NN
UK
[5]Department of Physiology, Anatomy, and Genetics
University of Oxford
South Parks Road
Oxford OX1 3PT
UK

Abbreviated title: Tracking of Labeled Stem Cells Seeded on PHA/PCL Scaffolds

Keywords: Polyhydroxyalkanoates, Polycaprolactone, Polymer Blends, Cardiac Progenitor Stem Cells, Polymer Scaffolds, ^{19}F Magnetic Resonance Spectroscopy/Imaging, Cardiac Regeneration.

Abstract

Medium-chain length Polyhydroxyalkanoates (MCL-PHAs) have demonstrated exceptional properties for cardiac tissue engineering (CTE) applications. Despite prior work on MCL-PHA/Polycaprolactone (PCL) blends, optimal scaffold production and use as an alternative delivery route for controlled release of seeded cardiac progenitor cells (CPCs) in CTE applications *in vivo* has been lacking. We present herein applicability of MCL-PHA/PCL (95/5 wt%) blends fabricated as thin films with an improved performance compared to the neat MCL-PHA.

Polymer characterization confirmed the chemical structure and composition of the synthesized scaffolds, while thermal, wettability, and mechanical properties were also investigated and compared in neat and porous counterparts. *In vitro* cytocompatibility studies were performed using perfluorocrown-ether (PFCE)-nanoparticle-labeled murine cardiac progenitor cells (CPC), and studied using confocal microscopy and ^{19}F MRS/MRI. Seeded scaffolds were implanted and studied in the post-mortem murine heart *in situ*, and in two additional C57BL/6 mice *in vivo* (using single-layered and double-layered scaffolds) and imaged immediately after and at 7 days post-implantation.

Superior MCL-PHA/PCL scaffold performance has been demonstrated compared to MCL-PHA through experimental comparisons of a) morphological data using scanning electron microscopy and b) contact angle measurements attesting to improved CPC adhesion, c) *in vitro* confocal microscopy showing increased SC proliferative capacity, d) mechanical testing that elicited good overall responses.

In vitro MRI results justify the increased seeding density, increased *in vitro* MRI signal, and improved MRI visibility *in vivo*, in the double-layered compared to the single-layered scaffolds. Histological evaluations (bright-field, cytoplasmic (Atto647) and nuclear (DAPI) stains) performed in conjunction with confocal microscopy imaging attest to CPC binding within the scaffold, subsequent release and migration to the neighboring myocardium, and to increased retention in the murine myocardium in the case of the double-layered scaffold.

Thus, MCL-PHA/PCL blends possess tremendous potential for controlled delivery of CPCs and for maximizing possible regeneration in myocardial infarction.

1. Introduction

Stem cell (SC) delivery has been proposed and applied as a novel and promising therapeutic approach for cardiac disease[1, 2, 3]. However, to-this-date, there is continued speculation over its efficacy, given the disparity of published preclinical and clinical results[4, 5], despite scientific evidence for the existence of paracrine effects associated with beneficial functional improvements in the infarcted myocardium[6]. Therefore, controlled SC administration and release still presents tremendous challenges towards a therapeutically successful cell engineering approach.

Polymer scaffolds have been introduced as a novel, biomimetic approach for administration and controlled release of viable SCs to the diseased myocardium[7], ultimately aiming to replace scar tissue with engrafted healthy cells with pluripotent/multipotent capacity.

Historically, the earliest attempts for tissue regeneration date to the early 1970s with the use of grafts over the injured myocardium[8]. The first efforts to deliver cells within scaffolds were pioneered by Souren *et al.*[9], while more recent attempts target the use of inducible pluripotent SCs[10].

To this-date, collective efforts in cardiac tissue engineering have employed natural and synthetic materials and have been tested with a multitude of SC types[8, 11] in different hosts, including the mouse, rat, rabbit, pig, sheep, dog, and human[8]. The scaffold substrates have been synthesized using materials, such as collagen, fibrin, chitosan, alginate[12], hyaluronic acid, gelatin, matrigel, decellularized extracellular matrix[13, 14], and hydrogels[15, 16].

In recent years, the scientific preference has shifted towards scaffolds synthesized using natural materials given their biodegradable and biocompatible properties, emulating closely the myocardial microenvironment. Specifically, medium-chain length polyhydroxyalkanoates (MCL-PHA) have generated great interest over recent years as functional materials in cardiac tissue engineering, with biodegradable, biocompatible, and synthetically tunable physical properties[17], including flexibility, crystallinity, melting point, and glass transition temperatures[18]. Induced porosity and functionalization of these materials with growth factors and active peptide molecules (without and with electrospun blend fibers) has also led to the fabrication of cardiac patches with excellent morphological properties, and upregulation of cues from the innate matrix structure, thereby promoting enhanced SC (endothelial, inducible pluripotent) adhesion and proliferation[17, 19]. Furthermore, MCL-PHA patches have been shown to exhibit similar mechanical properties to myocardial muscle, with a flexibility and rigidity that can sustain the cyclic strain patterns developed during the contractile-relaxation parts of the cardiac cycle, over prolonged periods that span multiple weeks[19]. In addition, these polymers exhibit degradation by surface erosion, leading to the maintenance of the scaffold's structure for a longer period of time, and hence provide better support functionality. Overall, MCL-PHAs are versatile, biocompatible, biodegradable, sustainable, display thermoplastic and elastomeric properties, and have predictable mechanical and physical characteristics[20]. They can be mass produced using controlled fermentations[21], and their biodegradation products are much less acidic (with hydroxyalkanoic acids as the main

degradation byproducts) as compared to those of PLLA and PLGA, thereby leading to less severe inflammatory responses. However, MCL-PHAa are associated with high production costs.

In comparison to MCL-PHAs, synthetic materials–such as poly(L-lactic acid) [PLLA][22] are readily available and are associated with well-established processing conditions, however, PLLA films are much stiffer than MCL-PHAs and exhibit poorer degradation responses (bulk erosion)[19], ultimately causing plastic deformation and failure during long-term exposure to cyclic strain[17]. Additionally, PLLA degradation products are acidic in nature, which ultimately leads to inflammation and to other undesirable reactions[23].

Polycaprolactone (PCL)[24] is an elastomeric synthetic polymer that is adaptable, versatile, produced in large scale, is associated with precise synthetic control using easily accessible materials, prolonged degradation time[25, 26], has good miscibility with various polymers, and possesses good and predictable mechanical and physical characteristics, often used in load-bearing tissues to enhance stiffness[25], although associated with very low glass transition and melting temperatures[27].

Despite these advantages, PCL is a non-sustainable polymer, and its production methods include solvent- and catalyst-based synthesis. In addition, PCL does not exhibit structural variability, and consequently, the resulting range of material properties exhibited by MCL-PHAs.

In view of these facts, polymeric MCL-PHA/PCL blends were used in this work to overcome the limitations of each of these polymer families, allowing the alteration of the mechanical properties of PCL, thereby enhancing the processability of the combined polymer product. Despite the existence of prior published work on MCL-PHA/PCL blends[28-32, 25, 26]**,** the reported compositions, aging, testing, and targeted applications have been distinctly different from this work, and they have not been previously used for cardiac tissue engineering applications in either unseeded or seeded forms.

Correspondingly, in this effort, we aimed to synthesize MCL-PHA/PCL blend scaffold compositions seeded for the first time with cardiac progenitor cells (CPCs) enhancing the elicited benefits by capitalizing on the advantages of each material class.

Critical to the successful administration and controlled release of SCs by the scaffold is our ability to monitor them noninvasively, particularly in a temporal manner[33]. Even though biolluminescence imaging (BLI) using reporter genes (such as luciferase) has allowed real-time, *in vivo* monitoring of viable SCs implanted on scaffolds[34], however, the spatial localization of the scaffold and its degradability pattern are not easily discernible.

In this work, we propose the use of novel, functional biodegradable, biocompatible natural/synthetic polymer blend scaffolds (comprised of MCL-PHA and PCL) to: a) benefit from the material properties of natural and synthetic polymers; b) achieve controlled delivery of homologous CPCs—previously shown to elicit beneficial functional effects (in the chronic phase) following acute, reperfused myocardial infarction (MI), in preclinical[6] and clinical studies[4]—thereby aiming to increase retention of delivered cells to the murine myocardium, c)

extend the temporal window over which the release of labeled CPCs is achieved compared to traditional direct injection techniques[35], and d) use ^{19}F MRI/MRS to noninvasively detect, and monitor the cells temporally.

The choice of the blend material underlies one of the important novelties of this work, given the increased ability of structural control in terms of its elastomeric nature and mechanical properties, the increased glass transition temperatures compared to neat PCL, and its potential to integrate with the myocardial network and be conjugated with bioactive molecules, such as vascular endothelial growth factor (VEGF) and Arg-Gly-Asp (RGD)/Tyr-Lle-Gly-Ser-Arg (YIGSR) peptides to further increase cellular attachment, viability, and proliferation[17, 19]. Another novelty relates to the visualization and monitoring of the repair process using ^{19}F MRI. The latter aim is pursued in a physiological model, despite the challenges of the low seeding density, cell dispersion, as these are governed by the small size of the murine heart, stringent anatomical limitations regarding the scaffold's placement, the endogenous hypoxic conditions, and the temporally dependent migration/dispersion of cells within the murine epicardium/mesocardium.

2. Experimental Procedures

2.1 Production of Poly-3-hydroxyalkanoates (PHAs)

2.1.1 Production of Medium Chain Length Polyhydroxyalkanoates

MCL-PHAs were produced by *Pseudomonas mendocina* CH50 using glucose as the sole carbon source under ~~a~~ nitrogen limiting conditions[36]. Batch fermentation was carried out in a 15 L bioreactor with an operating fermenter volume of 10 L. MCL-PHA production was completed in three stages:

a. Preparation of inoculum: A single colony of *P. mendocina* CH50 was used to inoculate sterile nutrient broth. The broth was incubated at 30^{o}C, at 200 revolutions per minute (rpm) for 16 h.

b. Preparation of second stage seed culture: The inoculum prepared at the first stage was used to inoculate a second stage mineral salt medium with glucose as the carbon source. It was incubated at 30^{o}C, at 200 rpm for 24 h.

c. Preparation and inoculation of production stage media: Prior to the inoculation of the production media, the fermenter was sterilized at 121^{o}C for 30 min. The sterile mixture of mineral salt medium (MSM), glucose, magnesium sulphate, and trace element solution, was aseptically added to the fermenter. The second stage seed culture was used to inoculate the production media. The culture was grown for a period of 48 h at 30^{o}C and at 200 rpm.

2.1.2 Extraction of MCL-PHA

The biomass was recovered by centrifuging the fermented cultures at a speed of 4600 rpm for approximately 45 min. The obtained biomass was lyophilized prior to extraction. MCL-PHA was extracted using the two-stage soxhlet extraction method. The powdered biomass was refluxed in methanol for 24 h to remove the impurities. The polymer was then extracted in chloroform for another 24 h. The solution was concentrated using a rotary vacuum evaporator and the polymer was precipitated using ice-cold methanol (1:10 polymer solution to ice-cold methanol).

2.2. Polymer Characterization

2.2.1 Chemical Characterization

Fourier Transform Infrared Spectroscopy (FTIR): FTIR analysis was also conducted using a Perkin-Elmer Spectrum Two Spectrophotometer, as described earlier[17].

Nuclear Magnetic Resonance (NMR): NMR was conducted on a 16.4T (700 MHz), high-field spectrometer (Bruker, Billerica, MA, USA) at University College, London. Samples were prepared in accordance to standard methodological procedures, as reported earlier[36, 37].

2.2.2 Thermal Characterisation

Thermal properties of the polymer, such as the melting temperature (T_m), and the glass transition temperature (T_g), were determined using a differential scanning calorimetry system (DSC, Model DSC 214, Polyma, Netzsch, Germany), equipped with an intra-cooler IC70 cooling system. A polymer sample (5 mg) was heated from –70 to 170^{o}C at a heating rate of 10^{o}C per minute over two successive heating-cooling cycles. The analysis was completed at the end of two heating cycles. DSC thermograms were analyzed using the Proteus 7.0 software.

2.2.3 Molecular Weight Analysis

The number average molecular weight, (M_n), and the weight average molecular weight, (M_w) of the polymer were determined using gel permeation chromatography (GPC, Model 1260 Infinity GPC, Agilent Technologies). The polymer solution (2 mg/mL) was introduced into the GPC system at a flow rate of 1 mL/min. The system was equipped with a 5 µm PLgel MIXED-C (300×7.5 mm) column calibrated using narrow molecular weight polystyrene standards from 162 Da to 15 kDa. The eluted polymer was detected with a refractive index detector. The data were analyzed using the Agilent GPC/SEC software.

2.3 Scaffold Synthesis and Characterization

MCL-PHA films were prepared using the solvent casting method[38]. Nonporous MCL-PHA films were prepared by dissolving the polymer (0.5 g) in chloroform (10 mL). The MCL-PHA solution was poured into a glass petri dish and was allowed to dry in a closed chamber. Polymer blends were prepared by dissolving 0.5 g of polymer with 0.26 g of PCL (Sigma-Aldrich, UK).

In order to prepare porous films, 1.7 g of sodium chloride particles of particular sizes (75, 100 μm) were used as porogens. These were added into the polymer solution, mixed, and then poured into glass petri dishes. Upon drying, these films were immersed in water to allow sodium chloride to leach out of the films[39, 40]. These films were dried in a closed chamber.
The basis for the ultimate choice of the 95/5 wt% MCL-PHA/PCL blend composition is attributed to the outcomes obtained from empirical optimization tests (at different blend compositions and porosities), and is based on previous work on PHA-based blends in relation to nerve tissue engineering using 95/5 wt% and 75/25 wt% MCL-PHA/PCL blends[41].

2.3.1 Mechanical Characterization

Mechanical properties of the porous and nonporous films were tested using an Instron tensile testing system (Instron, Model 5942 Testing Systems, Buckinghamshire, UK). This analysis was carried out on solvent cast film strips of specified widths and lengths (n=3, >10 mm in length and 5 mm in width). Tensile strength, elongation at break (%), and Young's Modulus values were determined from the stress–strain curve using the Instron's analysis package (BlueHill 3) or via offline analysis.

2.3.2 Morphological Properties

Surface properties of the porous and the nonporous films were studied using a JEOL 5610LV scanning electron microscope (SEM) (Hertfordshire, UK). MCL-PHA film samples were mounted on conducting aluminium stubs, and were coated with gold-platinum using an Emitech-K550 gold sputtering coater (Ashford, Kent, UK) for approximately 2 min before they were imaged using the SEM. The images were acquired using an acceleration voltage of 10 kV at a 10 cm working distance at the Eastman Dental Institute, University College, London.

2.3.3 Hydrophobicity-Contact Angle Measurements

Contact angle (θ) measurements were performed using a KSV Cam 200 optical contact angle measurement system (KSV Instruments Ltd.) on both porous as well as nonporous MCL-PHA films to determine their wettability. Distilled water and cell media (200 μL) were placed on the surface of the film sample using a gas tight syringe. Ten images of the water/media droplets dispersing on the surface of the film sample were captured within a frame interval of 1 s. The analyses of the images were performed using the KSV Cam software. All work was completed at the Eastman Dental Institute, University College, London.

2.4 Cardiac Progenitor Stem Cells

2.4.1 Isolation of Cardiac Progenitor Cells, Labeling, and Scaffold Seeding

Cell Isolation: CPCs were isolated from adult, C57BL/6, mouse atria. Specifically, after hearts were excised, they were washed, digested with 0.05% trypsin-EDTA, and the tissue explants were plated on fibronectin-coated petri dishes. They were expanded in culture as collagenase and trypsin digestion cells (CT) in accordance to standard methods described previously[42].

Labeling: Cells were then plated in Iscove's Modified Dulbecco's Medium (IMDM, Thermo Fisher Scientific, UK) and incubated in culture with Perfluoro-crown-ether (PFCE)-containing fluorescent nanoparticles (NPs) (containing Atto647) (10 mg/mL in 1 million cells)[43] and FuGENE^{HD} (Promega, Madison, WI, USA) for approximately 24 h before trypsinization, isolation, and pelleting. Final cell pellet suspensions containing approximately 1 million cells each were maintained in cell media solutions and transferred to Eppendorf volumes containing 1.7 mL IMDM. Labeled cells were used to seed the scaffolds for SEM, magnetic resonance imaging and spectroscopy (MRI/MRS), and confocal microscopy experiments.

Cell Seeding: Cells (unlabelled or labeled) were seeded on scaffolds overnight after isolation and pelleting. The seeding density was 20k/scaffold for confocal-epifluorescence imaging, and 300-500k/scaffold for *in vitro* MRI studies, with scaffolds cut at sizes spanning 2-8×2-8 mm^2. Scaffolds were subsequently washed with PBS (1:7 v/v), and fixed cells were seeded (in 2% paraformaldehyde (PFA) solution), while live cells were seeded in IMDM media. Scaffolds were subsequently prepared for high-content, confocal imaging, SEM, or for MRS.
In vivo scaffolds were cut into a trapezoidal shape (the smaller side was implanted towards the apex) with a size of 2×5 mm^2, with a height of 4 mm. The optimal seeding density was found to be 300-350k cells in 100 µm porous scaffolds (the ratio of the final number of cells to the number of the originally seeded cells was ~0.6). This estimate was based on in-vitro experiments where Trypan blue cell counts were conducted upon initial seeding/incubation, and corresponding counts of the freely floating cells in the IMDM media after the incubation period after the transfer of the scaffold in a new Eppendorf tube with fresh media. To maximize the cell density, a double-layered scaffold was implanted in a second mouse and studied *in vivo*, as reported below. The double-layered scaffold was composed of two single layer scaffolds that were glued at their four corners using surgical glue (Histoacryl, Braun Surgical S.A., Spain).

2.5 *In Vitro* Cell Adhesion and Proliferation Studies of Seeded Scaffolds

2.5.1 High-Content Microscopy-Epifluorescence Imaging

Epifluorescence Imaging: Live cells were stained with Calcein (CellTrace™ Calcein Red-Orange, ThermoFisher Scientific, UK) for high-content imaging, and plated in 96-well plates. Cells (n=3, ~20-50 k cells/well) were maintained in culture up to 7 d (D), and a time course study (D1-D7) of live cells was conducted to assess cell survival (Calcein) using a high-content imaging system (Operetta, Perkin-Elmer, UK) (results not shown).

Label Detection - Confocal microscopy

Fluorescent NPs were imaged [excitation wavelengths: λ_{green}=488 nm, λ_{red}=633 nm, emission ranges: 500-550 nm (green) and 650-700 nm (red)] using phase contrast, and red/green excitations in control cell samples, and in samples with and without FuGENE, using a Leica

TCS SP8 confocal microscope (Leica-Microsystems, Mainhem, UK) with HyD detectors, and an objective with numerical aperture (NA)=1.4, 63X.

2.6 *In Vitro*, Post-mortem, and *In Vivo* MRI/MRS

2.6.1 Animal Ethics

All experimental procedures involving animals were approved by the Home Office (UK) and were in accordance to the guidelines under The Animals (Scientific Procedures) Act, 1986, the European Animal Research Directive 2010/63/EU, and with local institutional guidelines.

2.6.2 Radiofrequency Coils

For MRI studies, a 4×4 cm^2 single-turn, transmit/receive butterfly coil (implemented on a 28 mm diameter plastic former) [*in vitro*/post-mortem/*in vivo* studies], and a 5 (diameter)×8 (length) mm^2 solenoid coil [*in vitro* studies], were fabricated in-house using flexible copper laminate sheaths, tuned, and matched to the ^{19}F resonant frequency at 375.8 MHz. The broad frequency response of the coil allowed intermittent imaging on the ^{1}H and ^{19}F nuclei.

2.6.3 MRI/MRS of Nonporous and Porous Scaffolds

In vitro studies: Unseeded and seeded scaffolds were maintained in IMDM media and placed in 0.2-0.7 mL Eppendorf tubes. ^{1}H and ^{19}F MRI/MRS were then conducted. For post-mortem studies, $^{1}H/^{19}F$ MRI were performed on hearts with control (unseeded) and labelled (seeded) scaffolds positioned using fibrin glue (Baxter, UK) on the anterior epicardial surfaces.

In vivo studies: Healthy mice were anesthetized and maintained using 1.5% isoflurane. They were then intubated and underwent a lateral thoracotomy. Scaffolds were positioned on the anterior myocardium using histoacryl surgical glue (B. Braun Surgical S.A., Spain). Mice were recovered, monitored for adequate post-surgical recovery, and transferred to MRI for imaging. They were then re-anesthetized in accordance to standard imaging protocols. Imaging parameters for all MRI/MRS acquisitions are listed below.

a) *In Vitro* Studies ^{1}H MRI (unseeded/seeded scaffolds): ^{1}H MRI was completed with two-dimensional (2D) segmented k-space, double-gated spoiled gradient echo (SPGR), and three-dimensional (3D) ungated sequences.

b) ^{19}F-MRI/MRS: Work was performed on a 9.4T Varian scanner. ^{19}F spectra were acquired using nonlocalized acquisitions (ungated and gated for *in vivo* scans) with the following parameters: repetition time (TR)=800-1000 ms, number of excitations (NEX)=64 or 256, 512 points, bandwidth (BW)=20 kHz, receiver gain (RG)=30.

c) *In Vitro* Studies ^{19}F MRI (unseeded/seeded scaffolds): Correspondingly, the ^{19}F MRI acquisitions (SPGR, steady state free precession (SSFP)) were: TR=8.3 ms, TE=4.17 ms, flip

angle=50°, NEX=1024, matrix=32×32, ST=10 and 40 mm, BW=4 kHz, RG=30, total acquisition time=4.3 min.

d) Post-mortem Studies (unseeded/seeded and labelled scaffolds): The 2D ^{1}H MRI acquisition parameters were: TR=2.73 or 3.13 ms, TE=1.58 ms, flip angle=50°, NEX=32, matrix=128×128. FOV=40x40 mm^2, ST=1 mm, BW=100 kHz, pw=1500 µs (total acquisition time = 12.8 s). The 3D ^{1}H MRI acquisition parameters were: TR=2.63 ms or 2.73 ms, TE=1.33 or 1.38 ms, flip angle=20°, NEX=4, matrix=128×128×128, FOV=40×40×40 mm^3, BW=100 kHz, total acquisition time=2.5 min.
The corresponding ^{19}F acquisition parameters were: TR=8.31 ms, TE=4.17 ms, flip angle=50°, NEX=796, matrix=32×32, ST=5 mm, BW=4 kHz, total acquisition time=3.31 min. ^{19}F MRS was acquired with nonselective excitation using TR=800 ms, NEX=256, 512 points, BW=20 kHz, RG=30.

e) *In Vivo* Murine Studies: 3D ungated scans were acquired using the following imaging parameters: TR=3 ms, TE=1.68 ms, flip angle=30°, NEX=4, matrix=128×128×128, FOV=40×40×40 mm^2, BW=100 kHz, total acquisition time =5 min.

2.7 Histology

2.7.1 Cellular Retention

Post-mortem histological evaluation was performed at D1 and D7 post-scaffold implantation to assess CPC retention. Mice were euthanized by cervical dislocation under general anesthesia and the hearts excised. The hearts were then dehydrated and fixed (either in a 15% sucrose, 0.4% PFA solution, or in a 4% PFA solution) after which they were embedded in paraffin and stored (at -80^{o}C or room temperature). Serial transverse paraffin sections of 10-17 µm were cut, from base to apex for histological staining using a nuclear stain 4', 6-diamidino-2-phenylindole (DAPI). Imaging and analyses were performed on a bright-field optical and on a confocal microscope (nuclear (DAPI), label (Atto647)).

2.8 Image Processing

2.8.1 Image and Spectral Analyses

Low-resolution ^{19}F MR images were imported and interpolated in ImageJ (NIH, Bethesda, USA) using bicubic splines to match the ^{1}H matrix size. Thoracic muscle ^{1}H and ^{19}F MRI were overlaid in ImageJ (opacity=40-70%). *In vitro* and *in vivo* spectra were read and processed in CSX (P. Barker-Kennedy Krieger Institute, Johns Hopkins USA) and using the interactive data language software (IDL, Harris Geospatial, USA). Signal and signal-to-noise ratio (SNR) values were estimated using standard methodologies[44].
High field polymer spectral processing was conducted using the Mnova software package (v12, Mestrelab Research, S.L., A Coruna, Spain). The chemical shifts were referenced

against the residual solvent signals at 7.26 ppm and 77.0 ppm for the ^{1}H and ^{13}C spectra, respectively.

2.9 Statistical Analyses

All results are reported as mean ± standard deviation (SD). Paired and unpaired, two-tailed Student's t-tests, were also used (XLSTAT, Addinsoft, New York) for mean comparisons (α=5%).

3. Results

3.1 Production of Poly(-3-hydroxyalkanoates) and physical characterization

The polymer was produced by the fermentation of *P. mendocina* CH50, purified, and structurally characterized, as previously described[36] (Figure 1). The concentration of the obtained biomass at the end of fermentation was 1.5 g/L. The final PHA concentration was 0.52 g/L.

3.1.1 FTIR and NMR

The polymer was identified to be MCL-PHA using FTIR. The two characteristic peaks of MCL-PHAs (1726.2 cm^{-1}, indicative of the ester carbonyl bond and 1160.0 cm^{-1}, indicative of C-O stretching) were present in the elicited FTIR spectrum. Final confirmation of the polymeric structure was carried out using ^{13}C and ^{1}H Nuclear Magnetic Resonance (NMR) spectroscopy (Figure 1 and Table 1). The observed ^{1}H NMR peak area ratios for the MCL-PHA were 2:1:2:8:3 (a: b: c: d, d*: e, e*), which exactly corresponded to the expected ratios from the structure, as shown in Figure 1B. The elicited ratio value of 8 obtained for the ^{1}Hs (annotated as d, d*) is the average of 6 and 10, that is, the number of protons in each monomeric unit type. In the case of the MCL-PHA/PCL blend, the polymeric peak ratios matched those of the pure MCL-PHA polymer. Hence, the MCL-PHA related peak area ratios were 2:1:2:8:3 (a: b: c: d, d*: e, e*), while those for the PCL were 1:2:1:1 (^a: ^b: ^c: ^d), as shown in Figure 1C.

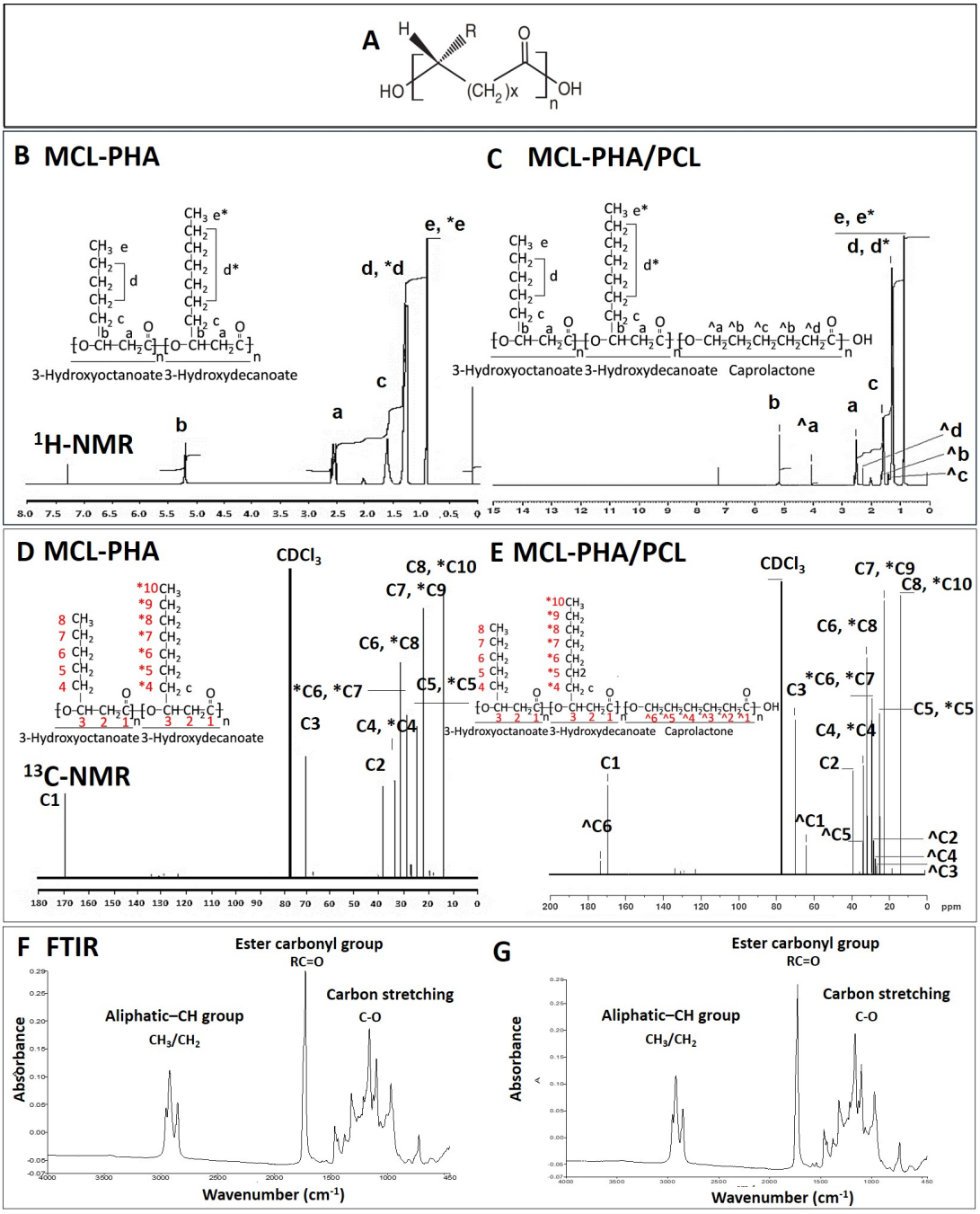

Figure 1: Synthetic and chemical characteristics of polymer: (A) General chemical structure of polyhydroxyalkanoates (x=1, 2, 3; n=100-30000; R_1, R_2=alkyl groups; C_1-C_{13} units). (B-E) NMR spectra of the MCL-PHA and MCL-PHA/PCL blend. (F, G) Corresponding FTIR spectra for MCL-PHA and MCL-PHA/PCL blend depicting the ester carbonyl bond and C-O stretching peaks. Only the characteristic peaks for PHAs and polycaprolactone are annotated in FTIR spectra[45, 46].

Table 1: Chemical shifts (δ) for (A) ^{1}H NMR peaks and corresponding chemical shifts for (B) ^{13}C peaks for MCL-PHA and caprolactone[37, 47].

(A)

Proton atoms	3-hydroxyoctanoate (δ, ppm)	Caprolactone (δ, ppm)
CH	5.20 (b, multiplet)	4.1 (^a, triplet adjacent to carbonyl group)
CH_2	2.50 (a, eightfold peak)	2.30 (^d, triplet)
CH_2	1.58 (c, multiplet)	1.65 (^b, eightfold peak)
Other CH_2	1.25 (d, d*, multiplet)	1.40 (^c, multiplet)
CH_3	0.88 (e, e*, triplet)	-

(B)

Chemical shift (δ, ppm)	3-hydroxyoctanoate	3- hydroxydecanoate	Caprolactone
173.0	-	-	^C6
170.0	C1	C1	-
70.0	C3	C3	-
64.0	-	-	^C1
40.0	C2	C2	-
34.0	C4	*C4	^C5
32.0	C6	*C8	-
30.0	-	*C6, *C7	-
28.0	-	-	^C2
25.0	C5	*C5	^C3
24.0	-	-	^C4
23.0	C7	*C9	-
14.0	C8	*C10	-

3.1.2 Thermal Properties

DSC was used to determine the thermal properties of the synthesized materials (Table 2). All thermograms showed the presence of two or more peaks corresponding to the melting and glass transition temperatures. T_g values for the MCL-PHA scaffolds (nonporous [n=4] and porous (75 [n=1]/100 μm [n=4]) at 100%) were -44.5/-44.0/-44.5^{o}C, while the corresponding values for the MCL-PHA/PCL blends (with PCL at 95/5%) were -48.2 (n=4)/-44.2 (n=1)/-46.5^{o}C (n=3). The corresponding T_m values were 52.1 (n=4)/53.2 (n=1)/53.6^{o}C (n=4) (100% composition) and 50.4 and 58.3/52.8 and 56.0/51.9 and 59.4^{o}C for the PCL blends. Two values are reported for the blends corresponding to the two distinct peaks elicited in the PCL blend thermograms.

Table 2: Summary of thermal characterization results of synthesized scaffolds.

Sample	Glass Transition (^{o}C)	Melting Temperature (^{o}C)
MCL-PHA (100%) Nonporous [n=4]	-44.5±1.6	52.1±0.4
MCL-PHA/PCL (95/5%) Nonporous [n=4]	-48.2±0.5	50.4±0.1/58.3±0.1[a]
MCL-PHA (100%) Porous (100 μm) [n=4]	-44.5±1.9	53.6±0.4
MCL-PHA/PCL (95/5%) Porous (100 μm) [n=3]	-46.5±1.1	51.9±0.1/59.4±0.3[a]

[a]Reported values correspond to the separate peaks of the MCL-PHA/PCL thermograms

3.1.3 Mechanical Properties

2D patches [nonporous and porous (75 and 100 μm porosity)] were fabricated using the solvent casting technique. Controlled porosity is a critical morphological characteristic for

biocompatible scaffolds for cell adhesion and growth. Therefore, porous patches were fabricated. The porosity was optimized based on the mechanical properties of the synthesized scaffolds (75, 100 μm), using tensile testing (Figure 2, Table 2).

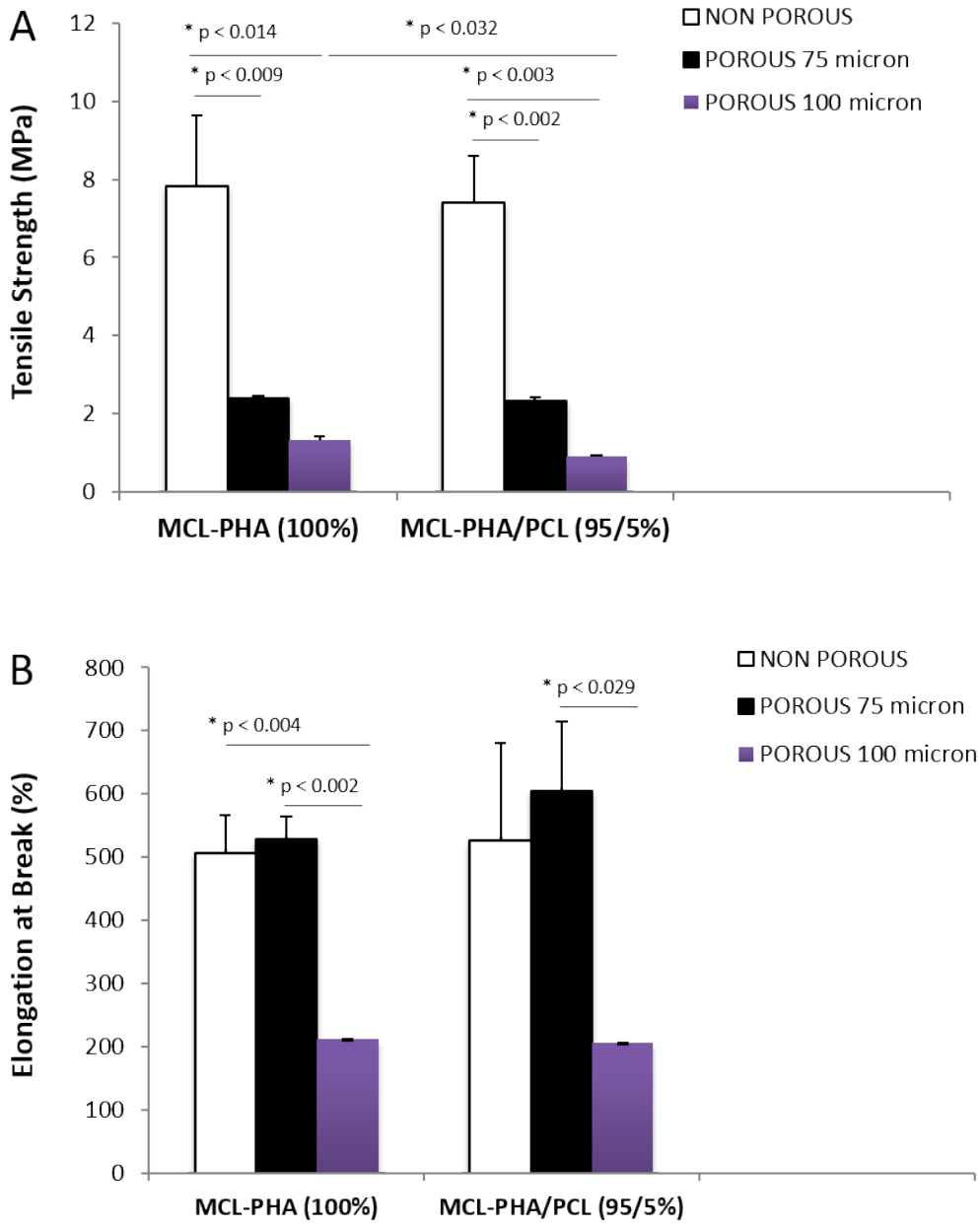

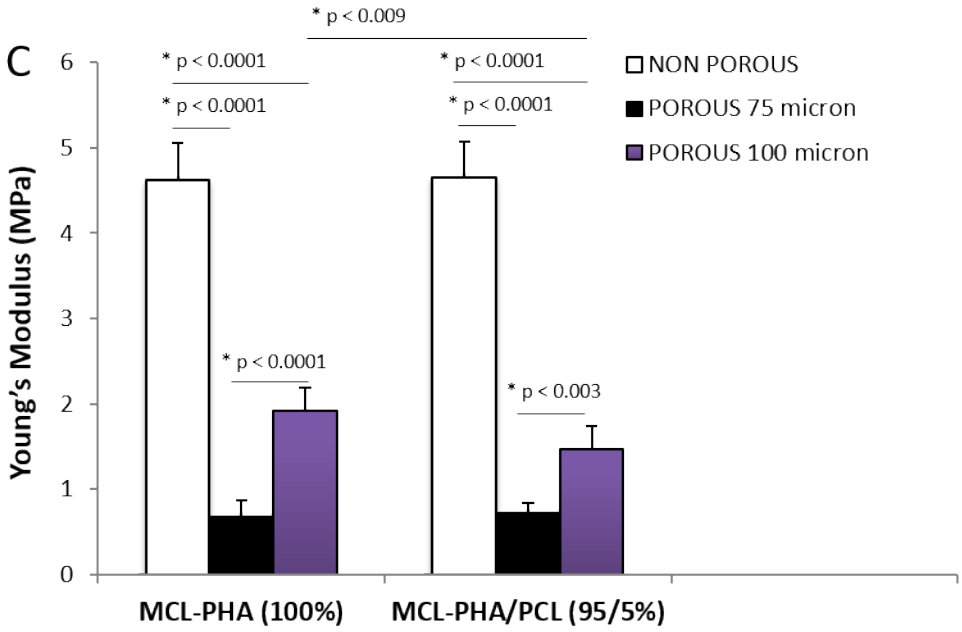

Figure 2: Mechanical characteristics of synthesized scaffolds: Histogram plots of (A) ultimate tensile strength (MPa), (B) elongation at break (%), and (C) Young's Modulus (MPa) for the nonporous (n=4), porous (75 μm [n=3], and 100 μm [n=7]) scaffolds. Results represent mean±sd values over 3-7 independent tests (Table 3).

Table 3: Summary of mechanical properties of synthesized scaffolds.

Sample	Tensile Strength (MPa)	Elongation at Break (%)	Young's Modulus (MPa)
MCL-PHA (100%) Nonporous	7.83	507.25	4.63
MCL-PHA/PCL (95/5%) Nonporous	7.40	526.50	4.65
MCL-PHA (100%) Porous (75 μm)	2.38	528.00	0.68
MCL-PHA (100%) Porous (100 μm)	1.31	212.50	1.92
MCL-PHA/PCL (95/5%) Porous (75 μm)	2.34	604.33	0.72
MCL-PHA/PCL (95/5%) Porous (100 μm)	0.91	206.00	1.46

3.2 Surface Characterization

The surface characteristics of the neat and porous scaffolds were quantified in terms of wettability and imaged using SEM. Surface morphology and microstructural features of the optimized porous scaffolds were visualized in cases of seeded scaffolds with CPCs using SEM, as shown in Figure 3.

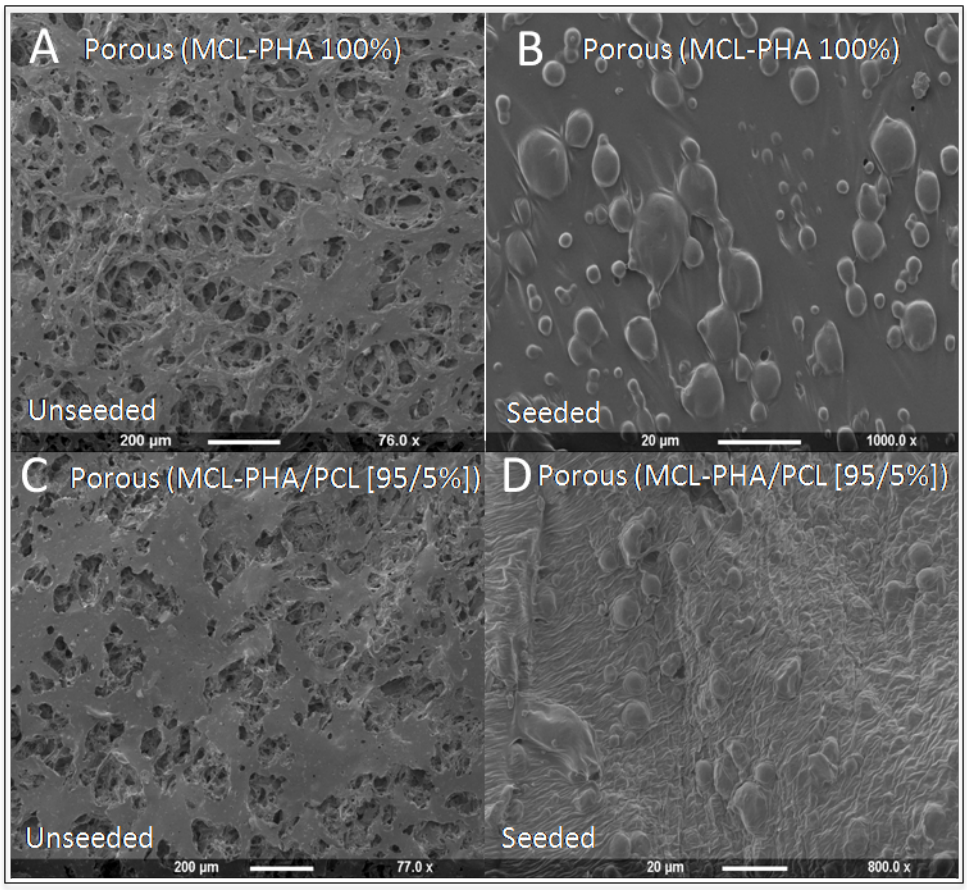

Figure 3: Surface morphology of porous scaffolds: Morphological characterization of synthesized (A, D) porous (MCL-PHA, MCL-PHA/PCL) scaffolds ((A, C) non-seeded, and (B, D) seeded with cardiac progenitor CT GFP-ve cells) using scanning electron microscopy. Indicative results are shown from the 75 µm porous scaffolds.

Surface wettability was quantified only for the neat scaffolds using water and IMDM media with a drop shape analyzer. The mean water contact angles for the nonporous scaffolds (MCL-PHA vs. MCL-PHA/PCL) were 90.0±11.6°/80.7±4.2° (water), and 88.8±6.7°/72.0±2.5° (IMDM), as shown in Figure 4. The contact angles were significantly ~~lower~~ higher in the H_2O vs. the IMDM cases (MCL-PHA: $p<0.013$, PCL: $p<0.015$). Significantly decreased mean contact angles were also observed in the MCL-PHA/PCL vs. MCL-PHA samples in the case of IMDM tests ($p<0.004$), indicative of increased hydrophilicity.

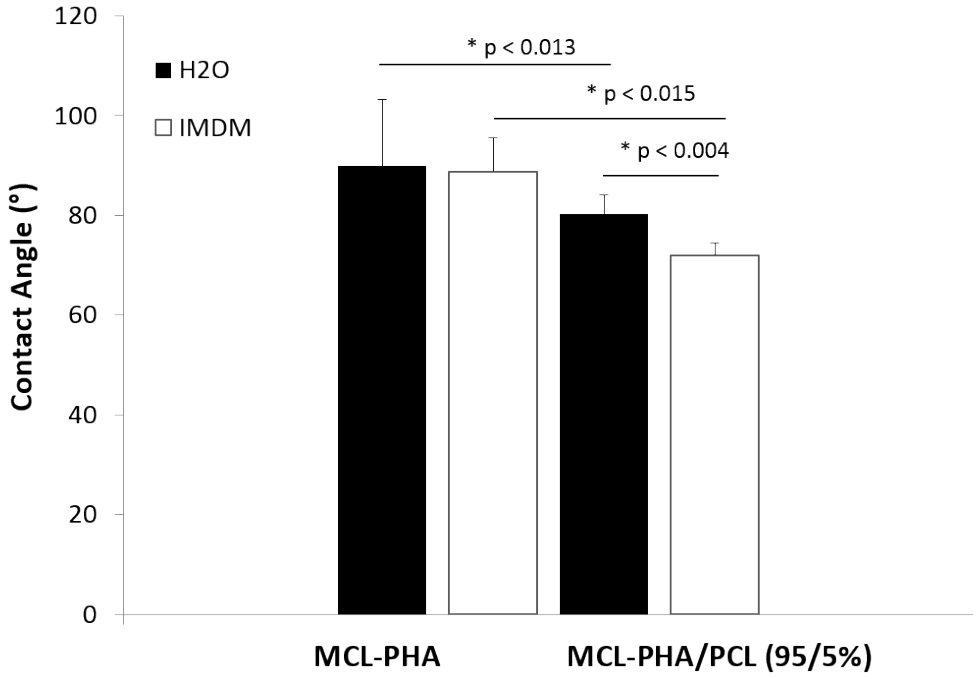

Figure 4: Contact angle measurements in synthesized scaffolds: Mean contact angles (mean±sd) over 6-11 independent measurements for three different samples of each of the synthesized scaffolds (neat MCL-PHA, and MCL-PHA/PCL blend at a composition of 95/5 wt%) using water and IMDM media.

3.3 Cardiomyocyte Cytocompatibility Studies

3.3.1 CPC Cell Density

The biocompatibility, cell surface adherence characteristics, and cell seeding density of the optimal porous scaffolds (with a porosity of 100 µm) were assessed using high-content epifluorescent imaging *in vitro*, using unlabeled and ^{19}F FuGENE-labeled cells (50-70k). The first set of experimental tests assessed the differences of cell adherences on the two types of the porous scaffolds having an optimal porosity of 100 µm. Elicited results are summarized in Figure 5 (A-B). Figure 5 clearly shows the increased cell adherence (and correspondingly increased viable cell density) in the MCL-PHA/PCL (Figure 5B) compared to the MCL-PHA neat scaffold (Figure 5, B). Quantification of the total number of viable cells was challenging given the 3D porous structure of the scaffold, and its optical scattering characteristics.

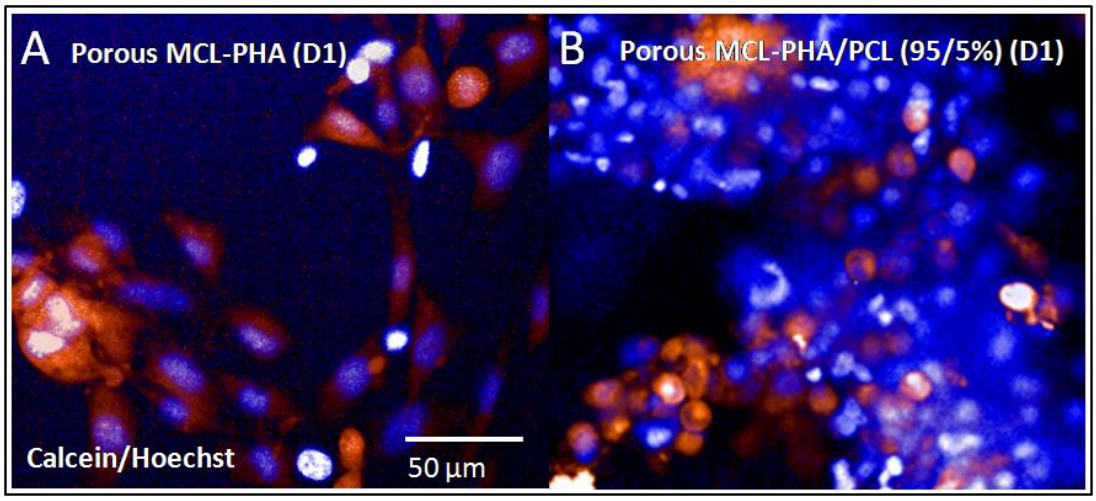

Figure 5: Comparison of *in vitro* CPC attachment on the two types of synthesized scaffolds: High-content (epifluorescent) imaging of porous MCL-PHA scaffolds (with a 100 µm porosity) seeded with (A) unlabelled (~50-70k cells) and CT cells [cytoplasmic Calcein stain (orange), nuclear Hoechst stain (blue)]. Results indicate the lower affinity of porous MCL-PHA scaffolds for unlabeled cardiac progenitor stem cells. (B) Increased cell density is observed for the porous MCL-PHA/PCL scaffold.

3.4 Noninvasive, Temporal Monitoring of Scaffolds using ^{19}F MRS/MRI

3.4.1 *In Vitro*, Post-mortem, and *In Vivo* Scaffold Characterization

Of increased interest are the MRS/MRI results from *in vitro* tests of the scaffold with optimal porosity (100 µm), summarized in Figures 6 and 7, over a temporal period of 9 days (D1-D9) following seeding with FUGENE-labeled cells. Constancy of cell retention is justified in Figure 6 by the 25% integrated MRS area difference between D1 and D3. The cell density decreased to 44% at D6 and to 30% at D9. MRI also achieved visualization and clear delineation of the scaffolds using both ^{1}H and ^{19}F MRI, as indicated in Figure 7. Indicative is the decreased signal (and SNR) responses at D6 compared to earlier days (Figure 7 G-I).

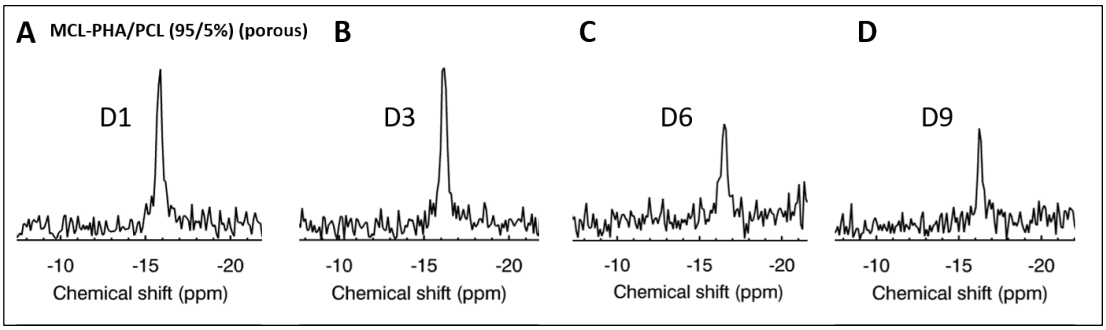

Figure 6: Temporal, *in vitro* MRS characterization of persistence of CPC attachment on the optimal type of porous scaffolds: Magnetic resonance ^{19}F spectra (MRS) of MCL-PHA/PCL (100 µm, 95/5%) scaffolds that were initially seeded with using 300k FuGENE-labeled CT cells each at (A-D) days 1 (D1), D3, D6, and D9.

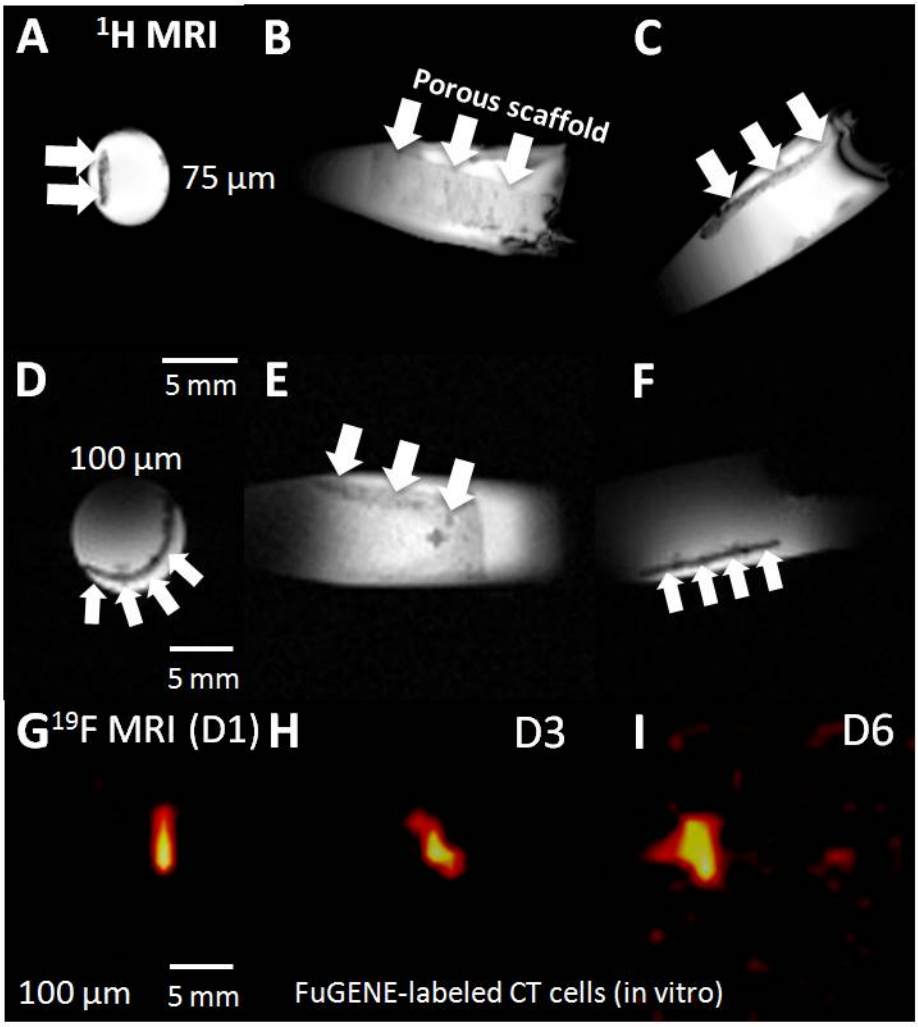

Figure 7: *In vitro* MR visualization and temporal monitoring of CPC seeded porous scaffolds: (A-C) Indicative axial (A) and coronal/sagittal (B, C) axis ^{1}H MRI views of a 75 µm porous MCL-PHA/PCL 95/5 wt% blend scaffold (arrows) showing *in vitro* detectability (samples immersed in IMDM media in 0.7 mL Eppendorf tubes). (D-F) Corresponding axis and coronal/sagittal views of a 100 µm porous scaffold *in vitro*. (G, I) ^{19}F MRI of seeded scaffold (MCL-PHA/PCL 95/5 wt% blend) with labeled cells. Axial views have a slice thickness of (G-I) 10 mm at D1, D3, and D6.

The seeded scaffolds were successfully tested in the post-mortem mouse using both ^{19}F MRS/MRI, as shown in Figure 8 (A-D). Results indicate responses at the first day following scaffold implantation. More interesting are the elicited results from the *in vivo* tests conducted in two C57BL/6 mice, indicating the ability of ^{19}F MRS to detect and track the labeled, seeded cells, within a week following initial implantation (Figure 8E-H). The two peaks on the left-most part of the PFCE-NPs represent the accumulated isoflurane peaks, as reported earlier[48]. The double-layered scaffold was also clearly and distinctly identified in ^{1}H MRI at D1 and D7 (the detected ^{19}F area doubled compared to the single-layered scaffold), as shown in Figures

8G, H. The single-layered scaffold was not visible using ^{19}F MRI as a result of the low seeding density (<300k at D1) [ultimately dependent on the scaffold's size in the case of the mouse], and the heterogeneous distribution of seeded cells within the scaffold, an effect that worsens owing to the rhythmic and cyclical contraction-relaxation pattern of the mouse heart at rates exceeding 350 beats per minute.

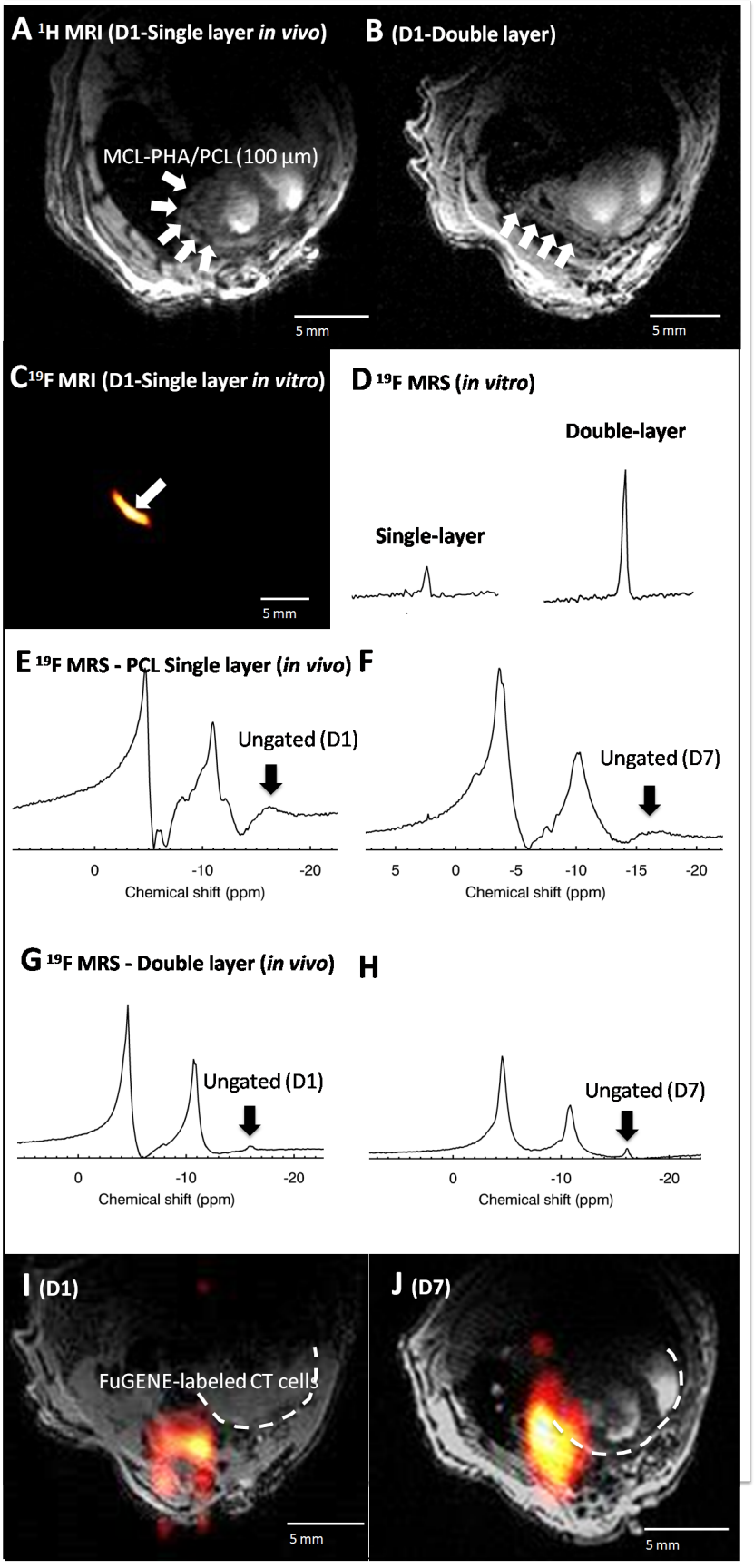
A ¹H MRI (D1-Single layer *in vivo*)
MCL-PHA/PCL (100 µm)
5 mm
B (D1-Double layer)
5 mm
C ¹⁹F MRI (D1-Single layer *in vitro*)
5 mm
D ¹⁹F MRS (*in vitro*)
Double-layer
Single-layer
E ¹⁹F MRS - PCL Single layer (*in vivo*)
Ungated (D1)
0
-10
-20
Chemical shift (ppm)
F
Ungated (D7)
5
0
-5
-10
-15
-20
Chemical shift (ppm)
G ¹⁹F MRS - Double layer (*in vivo*)
Ungated (D1)
0
-10
-20
Chemical shift (ppm)
H
Ungated (D7)
0
-10
-20
Chemical shift (ppm)
I (D1)
FuGENE-labeled CT cells
5 mm
J (D7)
5 mm

Figure 8: *In vivo* MR visualization and monitoring of signal responses from CPC seeded scaffolds: *In vivo* ^{1}H MRI of seeded scaffolds (with labelled CT cells) on the antero-lateral murine myocardium of normal C57BL/6 mice at day 1 (D1) from (A) single-layered and (B) double-layered porous MCL-PHA/PCL 95.5 wt% (100 µm) scaffolds seeded with FuGENE-labeled CT cells. (C) *In vitro* axial ^{19}F MRI of the single-layered scaffold. (D) *In vitro* comparison of single- and double-layered scaffolds using ^{19}F MRS, and (E-H) corresponding ungated ^{19}F MRS from the *in vivo* mouse (E, F) (single-layered scaffold), and (G, H) double-layered scaffold at D1 and D7. (I, J) Two separate axial views of the fused ^{1}H-^{19}F MRI of the double-layered scaffold at D1 and D7.

3.5 Histological characterization of implanted scaffolds

Figure 9 shows a histological short-axis, mid-apical view of the post-mortem heart indicating the sites of cellular migration and retention of CPCs within the myocardium and the scaffold. Also shown are the existing cellular entities at the interface of the scaffold and myocardium, as identified using bright field and confocal imaging (Atto647, DAPI).

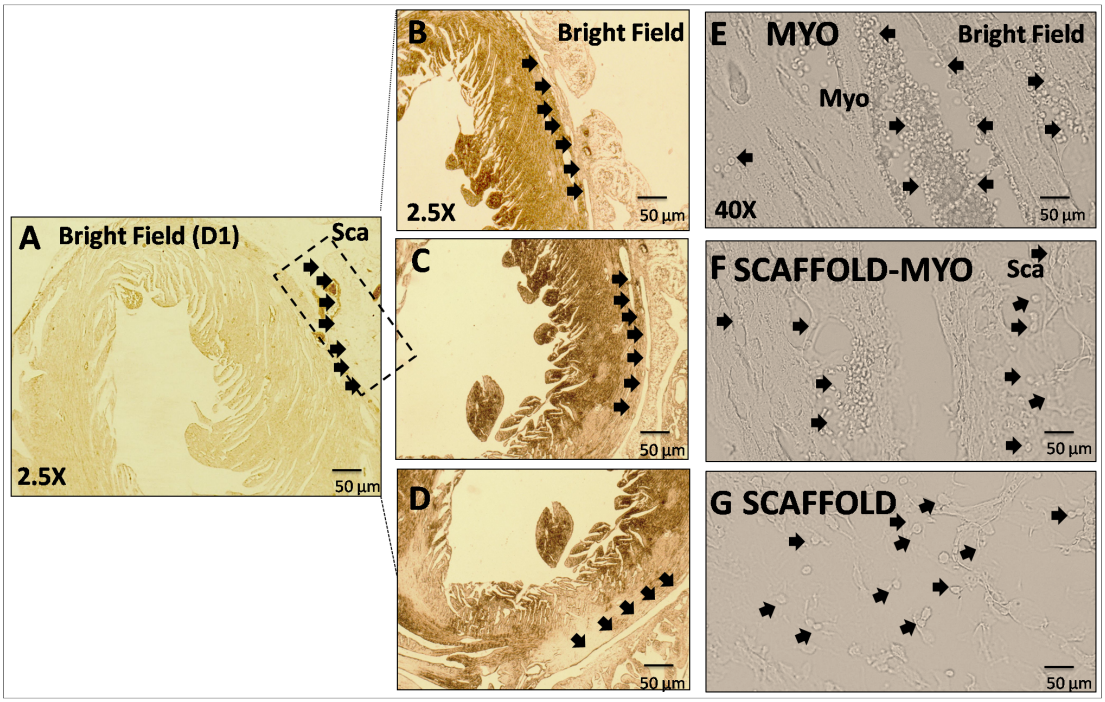

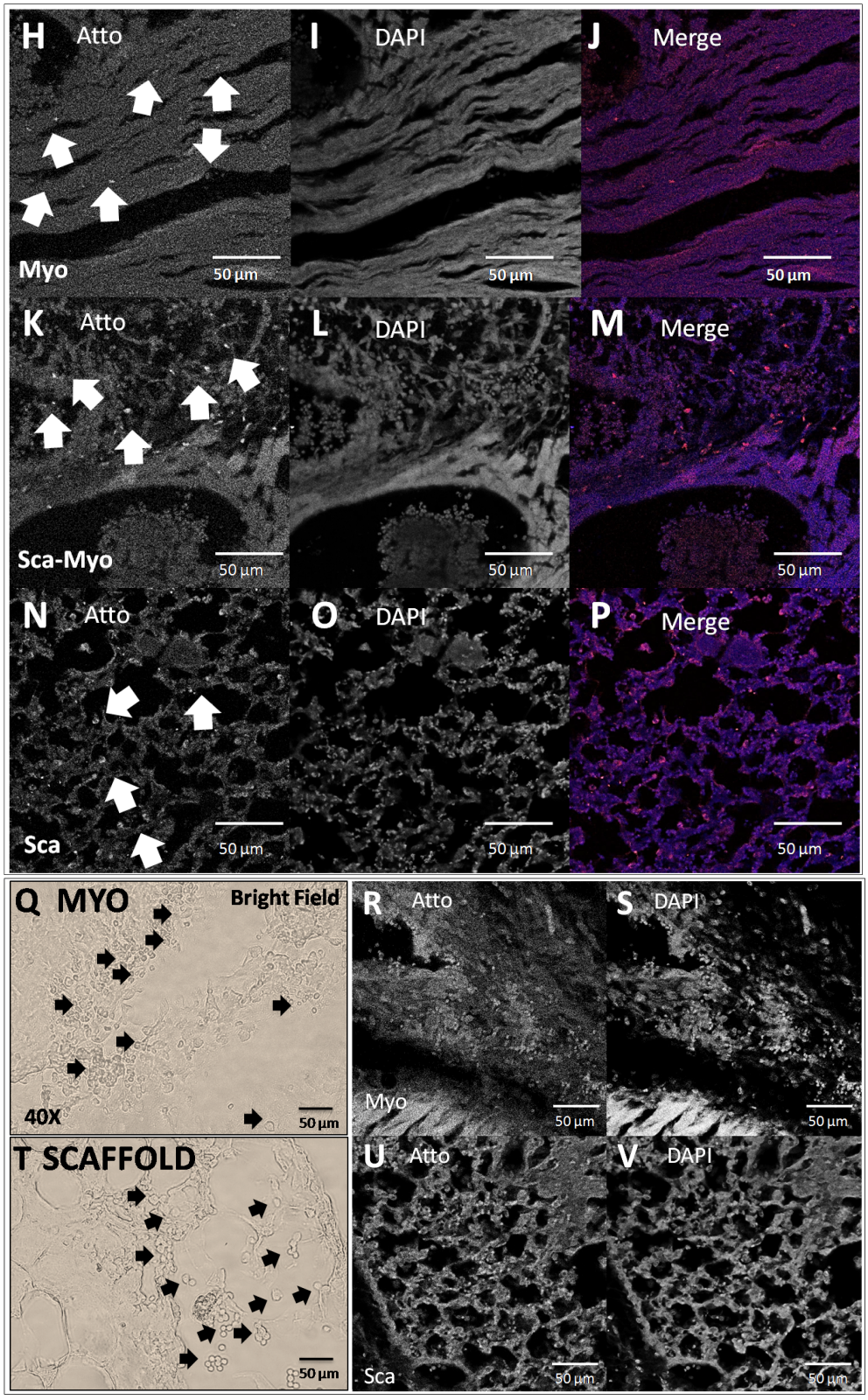

Figure 9: Histological assessment of single- and double-layered porous scaffolds seeded with CPCs: (A) Histological short-axis, mid-apical view of a fixed heart indicating the sites of scaffold (single layer) attachment, seeded scaffold cells, and cell retention of CPCs in the neighbouring myocardium. (B-D) Arrows in the middle and right sides of the subfigures indicate the locations of the scaffold and the scaffold-myocardial interface. (E-G) Black arrows

indicate the locations of detected cells (CPCs and red blood cells). (H-P) Shown also are fluorescent views (nuclear (DAPI), and label (Atto) presented in grayscale, and fused shown in color [Atto-red, DAPI-blue]), indicating CPC retention (H, K, N) within the scaffold and myocardium (white arrows). (Q-V) Corresponding histological and fluorescent views of the double-layered scaffold (shown in grayscale). Indicative is the increased number of cells within the myocardium compared to the single-layered case. Bright field images have been pseudocolored in different instances for better visualization.

4. Discussion

In this work, a novel, polymeric MCL-PHA/PCL blend material has been proposed for use as the substrate of a controlled delivery patch/scaffold for controlled SC release in cardiac tissue applications[16, 36]. Both MCL-PHA and MCL-PHA/PCL polymer types have been studied previously and have shown exceptional attributes to adhesion and cell proliferation for SCs[16, 18, 24]. In particular, MCL-PHAs have exhibited increased elastomeric responses, low crystallinity, low tensile strength, low melting points, and high elongations at break, and have been extensively studied in various applications to-date[49-51]. However, blend MCL-PHA/PCL compositions have not been explored previously for their suitability and responses in applications *in vivo* or for temporal imaging with CPCs. We show improved properties from synthesized scaffolds, capitalizing on the merits of each material class, as discussed below.

Chemical, Thermal, and Morphological Characteristics

The signaling interplay between the seeded CPCs on scaffolds and the local microenvironment have been shown to be deterministic for the cell fate, including migration, proliferation, differentiation, apoptosis, and/or homing/engraftment[6]. Correspondingly, the physical, morphological, and functional characteristics are deterministic for such responses.

Furthermore, the biocompatibility and degradability are essential to silence inflammatory/infectious responses, especially in cardiac disease. The scaffold's long-term stress/strain and thermoplastic responses are also critical in view of the cardiac cyclic activity.

DSC was used to assess the polymer's thermal properties, yielding (as previously shown) two distinct peaks corresponding to the T_g and T_m values observed within the ranges of 44–47^{o}C and 51–56^{o}C, respectively. Low glass transition and melting temperatures have a direct elastomeric impact on the material's response and are typical for MCL-PHA. Nevertheless, similar thermal properties were elicited for MCL-PHA and MCL-PHA/PCL blends that are most suitable for the proposed *in vivo* scaffold applications.

Porosity is also invariably linked with seeding density, and the ability of cells to inflitrate/cross-link, migrate, and for cell ingrowth (through maximization of the surface area and active binding sites). Despite pore size disparity, all samples (neat and blends at 95/5% compositions) were similar in pore and cellular morphology, thus confirming batch reproducibility.

A pore size of 100 μm was chosen, which is larger than the sizes of cells contained in the heterogeneous mixture of CPCs (endothelial, fibroblasts, innate cardiac SCs, spanning a size range of approximately 10-40 μm (mean pore size (±sd)=19.5±8.8 μm) in each spatial dimension. The porogen concentration used was optimal, in accordance to prior published work[17]. Smaller pore sizes are prohibitive for cellular seeding and permeation, while large pore sizes may prove detrimental to the scaffold's cell retention capacity.

Mechanical Characteristics

The scaffold's rigidity/flexibility is of upmost importance for eliciting proper functional responses (support for adhesion of seeded cells) and attaining a proper coupling constant[52] with the injured myocardium. Correspondingly, the ability to control, study, and quantify its mechanical characteristics is critical, and these attributes have been extensively investigated herein.

The constitutive law manifested in terms of the stress–strain response of the material is fully deterministic for its mechanical response under all operational conditions. To this effect, stress–strain was quantified for these membranes at room temperatures. No experimentation was conducted using membrane samples immersed in buffer solutions, although prior work has shown additional beneficial effects[17]. The decrease of the Young's Modulus values for the nonporous versus the porous counterparts was anticipated. Of importance is the noted decreasing trend for these values in the case of the blend scaffolds compared to the MCL-PHA counterparts as reported previously[53], indicative of a decreased stiffness. The documented disparity in the trend of Young's modulus values for scaffolds with targeted porosities of 75 μm and 100 μm is attributed to the actual pore size disparity (from targeted values) and increased pore size variability in these scaffolds. It is thus likely that the pore distributions in the two cases at the spatial scale of uniaxial tensile testing are similar.

The elongation at break and tensile strength were comparable for the neat and porous scaffolds, but significantly smaller in value compared to PCL constructs[54], and significantly higher than the reported ranges for human myocardium (100-300% for the elongation at break, and 3-15 kPa for tensile strength)[55, 56]. The achieved Young's Modulus values of the optimized (unseeded) porous scaffolds are high compared to targeted values of murine and human myocardium in the range of 0.02–0.5 MPa[17, 52, 54-56]. The stiffness of seeded scaffolds is anticipated to be even higher, exacerbating the scaffold-myocardium stiffness difference. While such property is fundamental in achieving an appropriate mechanical stiffness gradient between the patch and myocardium, the observed Young's modulus mismatch is not envisaged to be deleterious for the proposed applications. We not anticipate that an exact match is required for the scaffold to be effective. Instead, we consider the chemical gradient (owing to the concentration difference of free, mobile SCs in the scaffold and the endogenous pool of SCs in the innate myocardium) to be the most critical factor in facilitating an efficient diffusional-migratory SC process, especially in the case of the injured myocardium. Reinforcing these arguments is the fact that the stiffness of MI tissue (as previously

characterized using atomic force microscopy[56]) is greater than that of healthy myocardium (i.e., the stiffness mismatch is smaller). Correspondingly, the chemical gradient (increased SC density in scaffold versus lack of cells, or minimal number of recruited SC cells from the endogenous niche pool in MI tissue) is thus expected to be the predominant driving force for cell migration.

An additional advantage of the scaffold is that it can act as a passive restraint explant to provide mechanical support, or equivalently, act as a 'passive-assist construct', to counteract the induced stress from the myocardial pressure-overload during remodeling in reperfused MI. The beneficial characteristics of the scaffold as a possible passive-assist explant are anticipated to be highly effective in the case of MI, whereby the load restraint imposed by the attached patch is expected to ameliorate and offset the dilatatory and hypertrophic response of the injured myocardium, elicited in the acute (dilation), and chronic MI phases (connective tissue deposition and scar formation) that ultimately lead to heart failure. The elongation at break and ultimate tensile strength characteristics were also within expected operational limits for both healthy and diseased states[17, 19]. Of increased importance are perhaps the surface characteristics of the scaffold, as described next.

Surface Characterization

The material's roughness and hydrophobicity are critical markers relevant to cellular adhesion and proliferation[16]. The surface roughness of this MCL-PHA was reported previously based on light interferometric techniques and measurements[17, 19] with a noted increase in the case of porous versus neat patches.

SEM and surface contact analyses revealed that both the neat and non-porous blend films had smooth, and regular surfaces, and that the specific cardiac myocytes adhere well on the outer surfaces of the non-porous scaffolds.

Given that the measured contact angles were 90° or less, both material types are considered as hydrophilic. As expected, there was an increased surface hydrophilicity with the use of IMDM, an effect that is more prominent in the MCL-PHA/PCL blends compared to the MCL-PHA scaffolds. This is expected as a result of the content of such media in electrolytes and other proteins that facilitate surface binding and adhesion. Surface contact angle results (IMDM vs. H_2O) have also been justified by SEM analyses indicating good outer surface adherence of CPCs in both cases (neat and porous). More importantly, increased hydrophilicity was documented in the case of neat MCL-PHA/PCL scaffolds compared to their MCL-PHA counterparts, confirmed by the excellent CPC attachment and increased retention, as shown by confocal microscopy and ^{19}F MRS findings. Further hydrophilicity increases are expected from the functionalization of these scaffolds with VEGF and RGD/YIGSR peptides[17].

Novel Functional Response in Cardiac Tissue Engineering

Cell Retention, ^{19}F Temporal Persistence, and Noninvasive Monitoring

The material has been synthesized to attain optimal characteristics (including pore size, actual physical dimensions, biochemical composition) to tailor its physical, chemical, thermal characteristics, and to optimize the seeding density of CPCs with fluorinated NPs for visualization and temporal tracking using MRS over periods spanning >7-9 days.

The pore size of the scaffold has been chosen to be large enough to accommodate all different types of cells contained in the heterogeneous population of the seeded CPCs (including primarily innate myocardial, endothelial cells, and fibroblasts), yet being able to accommodate other types of cardiac stem cells (e.g., mesenchymal, embryonic, inducible-pluripotent, and others).

The scaffold's seeding density (limited capacity determined by pore size, thickness, and size of patch ultimately limited by the murine myocardium) is approximately 350 k cells/scaffold, which is at the limit of the capacity of ^{19}F MRI to detect and monitor labeled cells using fast imaging with the described imaging methodologies at 9.4T.

Overall, SC retention has been proven, yet the cellular attachment can be further improved using VEGF/RGD/YIGSR. Nevertheless, the ability to maintain cells viable over multiple weeks is/will continue to be a challenge, as will be the determination on whether the increased ^{19}F signal observed at later time periods using the double-layered scaffold is due to released NPs from lysed cells within the pouch region between the two layers.

Temporal-dependent ^{19}F MRI decreases from seeded scaffolds, likely attributed to cell death, decreased cell adherence, and increased leaching rates of nonviable and viable cells, need to be investigated further. Conclusive confirmation is envisaged to be provided by *in vitro* dead/live assays and post-mortem immunohistochemical assays following *in vivo* imaging, as part of future planned work.

The engraftment also needs to be assessed once the optimal scaffold conditions are attained over periods of 1-8 weeks to assess N-cadherin, connexin43, and spatial gap junction formation and localization within the intercalated disc[58]. Although the exact mechanisms through which scaffolds exert beneficial effects are still not well understood, it is likely that they promote neogenesis and angiogenesis in conjunction with an associated increased SC viability and proliferation, amplifying the beneficial paracrine effects.

Overall, the elicited results from prior and ongoing clinical trials and preclinical studies of CPCs and SCs have been promising. Nevertheless, despite the existence of vast prior work in this field, important questions still remain, including the optimal choice of cells, growth factors, the scaffold's mechanical coupling and directionality of the explants with respect to the injured myocardium[58], and the exact timing of its administration after MI in order to elicit maximum benefits[59].

Conclusions

We have presented applicability of MCL-PHA/PCL porous blends fabricated as thin films with an improved performance compared to MCL-PHAs, capitalizing on the excellent polymeric properties of natural MCL-PHA polymers, and the simplified synthetic process relevant to

PCLs. We have also demonstrated superior MCL-PHA/PCL scaffold performance compared to MCL-PHA scaffolds through experimental comparisons of a) morphological data using SEM and b) contact angle measurements indicative of increased hydrophilic responses of the blend scaffolds attesting to improved CPC adhesion, c) *in vitro* confocal microscopy showing increased SC proliferative capacity, d) mechanical testing that elicited good overall responses, e) improved *in vitro* NMR retention of seeded SCs, and f) and *in vivo* applicability and MRI visualization of labeled SCs over periods spanning 8 days. The scaffold's structural and morphological characteristics are tunable and could allow maximization of the seeding density for easier detection and temporal follow-up using direct ^{19}F MRI/MRS *in vivo*, anticipated to be beneficial to larger animals/humans. The proposed scaffold can be potentially modified synthetically to address the induced CPC hypoxic state post-scaffold implantation through the controlled delivery of exogenously administered oxygen via the scaffold, particularly following MI, as a result of the loss of perfusion pathways and myocardial vascular obstruction (MVO) effects. Additionally, conjugation/functionalization of the scaffold with angiogenic, vascular growth factors, and peptides, is possible, and is expected to lead to even further increases in cellular attachment and proliferation, as evidenced previously in MCL-PHA seeded with other SC types[17].

Based on this work, and the elicited preclinical outcomes in normal mice *in vivo*, MCL-PHA/PCL blends are expected to have tremendous potential as future materials for cardiac patch development. A dual approach combining direct injections and controlled delivery of CPCs using these scaffolds is expected to maximize potential benefits following infarction. For translational purposes, refinement of the synthetic method of patch production is also envisaged, whereby the automation of the processing of polymeric synthesis and its direct, in situ injection can be implemented in accordance to recently published studies[60, 61]. Studies on their suitability and effects on MI are ongoing.

Acknowledgements

We are thankful to Ms. A. Vernet for her help with the *in vivo* studies, Dr. M. Maguire for the permission to use the solenoid coil for some of the in vitro studies, and Dr. A. Shaw for his help with the histological imaging. We thank Professor Jonathan Knowles for providing access to the contact angle measurement and SEM facilities at the Eastman Dental Institute and surgeon Dr. A. Achilleos at the Mediterranean Medical Center, Limassol, Cyprus, for his help with the surgical glue.

Conflicts of Interest

None.

Funding Sources

The work was supported by the European Union's Horizon 2020 research and innovation programme under the Marie Sklodowska-Curie [grant agreement No. 652986], the European Research Council Grant ERC-2013-StG-336454 (MS), and the Wellcome Trust Core Award [grant 090532/Z/09/Z]. Funding was also provided by the ReBioStent project – European Union's Seventh Programme for research, technological development and demonstration under grant agreement No. 604251 (PB, BL), and by the Neurimp project under grant agreement No. 604450 (PB). QAM is funded by a National Heart and Lung Institute Scholarship.

Contributors

The contributions of the authors of this article are:

a) Participation in the research: CC, PB, BL, RC, CAC, IR, QAM, ES (NP synthesis)
b) Article preparation: CC, PB, BL, RC, CAC, MS, IR
c) Design of experiments: CC, PB, BL, IR
d) Data collection: CC, PB, QAM, BL
e) Data analysis and interpretation: CC, PB, BL, RC, QAM, CAC, IR
f) Compilation of the article: CC, PB, BL, CAC, IR
g) Approval of the final version of the article: CC, PB, BL, RC, MS, QAM, ES, CAC, IR

Disclosure

All authors have approved the final article.

Role of the Funding Source

The funding sources had no involvement/role in the decision to submit the article for publication, or for the conduct of the research and/or the preparation of the article as such pertains to the categories (a-g) listed above.

References

1. Chamuleau, S.A.J; Vrijsen, K.R.; Rokosh, D. G.; Tang, X.L.; Pick, J.J.; Bolli, R.; Cell Therapy for Ischaemic Heart Disease: Focus on the Role of Resident Cardiac Stem Cells. Neth Heart J **2009**, *17*, 199–207.

2. Beltrami, A.P.; Barlucchi, L.; Torella, D.; Baker, M.; Federica, L.; Chimenti, S.; Kasahara, H.; Rota, M.; Musso, E.; Urbanek, K.; Leri, A.; Kajstura, J.; Nadal-Ginard, B.; Anversa, P. Adult Cardiac Stem Cells are Multipotent and Support Myocardial Regeneration. Cell **2003**, *114*, 763–776.

3. Oh H, Bradfute, S.B.; Gallardo, T.D.; Nakamura, T.; Gaussin, V.; Mishina, Y.; Pocius, J.; Michael, L.H.; Behringer, R.R.; Garry D. J.; Entman, M.L.; Schneider, M.D. Cardiac Progenitor Cells from Adult Myocardium: Homing, Differentiation, and Fusion after Infarction. Proceedings of the National Academy of Sciences **2003**, *100*, 12313–12318.

4. Malliaras, K.; Marban, E. Cardiac Cell Therapy: Where We've Been, Where We Are, and Where We Should be Headed. Br Med Bull **2011**, *98*, 161–185.

5. Zhu, W.Z.; Hauch, K.; Xu, C.; Laflamme, M.A. Human Embryonic Stem Cells and Cardiac Repair. Transplant Rev **2009**, *23*, 53–68.

6. Carr, C.; Stuckey, D.J.; Tan, J.J.; Tan, S.C.; Gomes, R.S.M.; Camelliti, P.; Messina, E.; Giacomello, A.; Ellison, G.M.; Clarke, K. Cardiosphere-derived Cells Improve Function in the Infarcted Rat Heart for at Least 16 weeks-an MRI Study. PLoS One **2011**, *6*, e25669.

7. Li, R.K.; Jia, Z.Q.; Weisel, Mickle, D.A.; Choi, A.; Yau, T.M. Survival and Function of Bioengineered Cardiac Grafts. Circulation **1999**, *100* (Suppl II), 63–69.

8. Perea-Gill, I.; Prat-Vidal, C.; Bayes-Genis, A. In Vivo Experience with Natural Scaffolds for Myocardial Infarction: the Times they are Changing. Stem Cell Research and Therapy **2015**, *6*, 248.

9. Souren, J.E.; Schneijdenberg, C.; Verkeij, A.J.; Van Wijk, R. Factors Controlling the Rhythmic Contraction of Collagen Gels by Neonatal Heart Cells. In Vitro Cell Dev Biol **1992**, *28*, 199–204.

10. Ye, L.; Chang, Y.H.; Xiong, Q.; Zhang, P.; Zhang, L.; Somasundaram P.; Lepley, M; Swingen, C; Su, L; Wendel, J.S.; Guo, J.; Jang, A.; Rosenbush, D.; Greder, L.; Dutton, J.R.; Zhang, J.; Kamp, T.J.; Kaufman, D.S.; Ge, Y.; Zhang, J. Cardiac Repair in a Porcine Model of Acute Myocardial Infarction with Human Induced Pluripotent Stem Cell-derived Cardiovascular Cells. Cell Stem Cell **2014**, *15*, 750–761.

11. Howard, D.; Buttery, L.D.; Shaesheff, K.M.; Roberts S.J. Tissue Engineering: Strategies, Stem Cells and Scaffolds Journal of Anatomy **2008**, *213*, 66–72.

12. Dar, A.; Schochar, M.; Leor, J.; Cohen. S. Optimization of Cardiac Cell Seeding and Distribution in 3D porous Alginate Scaffolds. Biotechnology Bioengineering **2007**, *80*, 305–317.

13. Bible, E.; Dell'Acqua, F.; Solanky, B.; Balducci, A; Crapo, P.M.; Badylak, S.F.; Ahrens, E.T.; Modo, M. Non-invasive Imaging of Transplanted Human Neural Stem Cells and ECM

Scaffold Remodelling in the Stroke-damaged Rat Brain by ^{19}F- and diffusion-MRI. Biomaterials **2012**, *33*, 2858–2871.

14. Casper, D.H.; Theisen, J.M.; Moreno, A.P.; Warren, M.; Silva, F.; Grainger, D.W.; Bull, D.A.; Patel, A.N. Novel Xeno-free Human Heart Matrix-derived Three-dimensional Scaffolds. Journal of Translational Medicine **2015**, *13*, 194–208.

15. Kraehenbuehl, T.P.; Ferreira, L.S.; Hayward, A.M.; Nahrendorf, N.; van der Vlies, A.J.; Vasile, E.; Weissleder, R.; Langer, R.; Hubbell, J.A. Human Embryonic Stem Cell-derived Microvascular Grafts for Cardiac Tissue Preservation after Myocardial Infarction. Biomaterials **2011**, *32*, 1102–1109.

16. Gishto, A.; Farrell, K.; Kothapalli, C.R. Tuning Composition and Architecture of Biomimetic Scaffolds for Enhanced Matrix Synthesis by Murine Cardiomyocytes. Journal of Biomedical Materials Research A **2015**, *103A*, 693–708.

17. Bagdadi, A.V.; Safari, M.; Dubey, P.; Basnett, P.; Sofocleous, P.; Humphrey, E.; Lacke, I; Edirisinghe, M.; Rrrocciano, C.; Boccaccini, A.R.; Knowles, J.C.; Harding, S.E.; Roy I. Poly(3-hydroxyoctanoate), a Promising New Material for Cardiac Tissue Engineering. J Tissue Eng Regen Med. **2018**, *12,* e495–e512, DOI: 10.1002/term.2318.

18. Volova T.G. *Polyhydroxyalkanoates--plastic Materials of the 21st Century: Production, Properties, Applications*; Nova publishers: New York, 2004.

19. Dubey P. Development of Cardiac Patches using Medium Chain Length Polyhydroxyalkanoates for Cardiac Tissue Engineering. Ph.D. Thesis, U. Westminster, London, England, 2017.

20. Keshavarz, T.; Roy, I. Polyhydroxyalkanoates: Bioplastics with a Green Agenda. Current Opinion in Microbiology **2010**, *13*, 321–326.

21. Roy, I.; Sivaniah, E.; Summers, D.; Thomson, N. In Vitro Production of Polyhydroxyalkanoates: Achievements and Applications. Journal of Chemical Technology and Biotechnology **2010**, *85*, 760–767.

22. Liu, Q.; Tian, S.; Zhao, C; Chen, X.; Lei, I.; Wang, Z.; Ma, P.X. Porous Nanofibrous Poly(L-lactic acid) Scaffolds Supporting Cardiovascular Progenitor Cells for Cardiac Tissue Engineering. Acta Biomaterialia **2015**, *26*, 105–114.

23. Li, H.; Chang, J. Preparation and Characterization of Bioactive and Biodegradable Wollastonite/Poly (D, L-lactic acid) Composite Scaffolds. Journal of Materials Science: Materials in Medicine **2004**, *15*, 1089–1095.

24. Miyagi, Y.; Zeng, F.; Huang, X.P.; Foltz, W.D.; Wu, J.; Mihic, A.; Yau, T.M.; Weisel, R.D.; Li, R.K. Surgical Ventricular Restoration with a Cell- and Cytokine-seeded Biodegradable Scaffold. Biomaterials 2010, *31*, 7684–7694.

25, Malikmammadov, E.; Tanir, T.E.; Kiziltay, A.; Hasirci, V.; Hasirci, N. PCL and PCL-based Materials in Biomedical Applications. Journal of Biomaterial Science Polymer Edition **2018**, *29*, 8680893.

26. Tang, Z. G.; Black, R. A.; Curran, J. M.; Hunt, J. A.; Rhodes, N. P.; Williams, D. F. Surface Properties and Biocompatibility of Solvent-case Poly[ε-caprolactone] Films. Biomaterials **2004**, *25*, 4741–4748.

27. Adhikari, R.; Gunatillake, P.A. Biodegradabel Synthetic Polymers for Tissue Engineering. European Cells and Materials **2003**, *5*, 1–16.

28. Duarte, M. A. T.; Hugen, R. G.; Martins, E. S. A. Thermal and Mechanical Behavior of Injection Molded Poly(3-hydroxybutyrate)/Poly(ε-caprolactone) Blends. Materials Research **2006**, *9*, 25–27.

29. Garcia-Garcia, D.; Ferri, J. M.; Boronat, T.; Lopez-Martinez, J.; Balart, R. Processing and Characterization of Binary Poly(hydroxybutyrate) (PHB) and Poly(caprolactone) (PCL) Blends with Improved Impact Properties. Polymer Bulletin **2016**, *73*, 3333–3350.

30. Katsumata, K.; Saito, T.; Yu, F.; Nakamura, N.; Inoue, Y. The Toughening Effect of a Small Amount of Poly(ε-caprolactone) on the Mechanical Properties of the Poly(3-hydroxybutyrate-co-3-hydroxyhexanoate)/PCL Blend. Polymer Journal **2011**, *43*, 484–492.

31. Guarino, V.; Alvarez-Perez, M.; Ambrosio, B. C. L. hMSC Interaction with PCL and PCL/Gelatine Platforms: A Comparative Study on Films and Electrospun Membranes. Journal of Bioactive and Compatible Polymers **2011**, *26*, 144–160.

32. Li, Z.; Yang, J.; Loh X. J. Polyhydroxyalkanoates: Opening Doors for a Sustainable Future. NPG Asia Materials **2016**, *8*, e265–e284.

33. Terrovitis, J.V.; Bulte, J.W.M.; Savvanathan, S.; Crowe, L.A.; Savathchandra, P.; Batten, P.; Sachlos, E.; Chester, A.H.; Czernuszka, J.T.; Firmin, D.F.; Taylor, P.M.; Yacoub, M.H. Magnetic Resonance Imaging of Ferumoxide-labeled Mesenchymal Stem Cells Seeded on Collagen Scaffolds-relevance to Tissue Engineering. Tissue Engineering **2006**, *12*, 2765–2775.

34. Hwang, D.W.; Jang, S.J.; Kim, Y.H.; Kim, H.J.; Shim, I.K.; Jeong, J.M.; Chung, J-K.; Le, M.C.; Lee, S.J.; Kim, S.U.; Kim, S.; Lee, D.S. Real-time In Vivo Monitoring of Viable Stem Cells Implanted on Biocompatible Scaffolds. Eur J Nucl Med Mol Imaging **2008**, *35*, 1887–1898. doi: 10.1007/s00259-008-0751-z.

35. Constantinides, C; Maguire, M; Carnicer, R; Swider, E; Srinivas, M; Carr, M. A.; Schneider, J. S. Fast, Quantitative, Murine Cardiac ^{19}F MRI/MRS of PFCE-labeled Progenitor Stem Cells and Macrophages at 9.4T. PLoS One **2018**, *13*, e0190558.

36. Rai, R.; Keshavarz, T.; Roether, J.A.; Boccaccini, A.R.; Roy, I. Medium Chain Length Polyhydroxyalkanoates, Promising New Biomedical Materials for the Future. Materials Science and Engineering **2011**, *72*, 29–47.

37. Basnett, P.; Lukasiewicz, B.; Marcello, E.; Kaur, H.; Knowles J. C.; Roy, I. Production of a Novel Medium Chain Length Poly(3-hydroxyalkanoate) using Unprocessed Biodiesel Waste and its Evaluation as a Tissue Engineering Scaffold. Microbiology Biotechnology **2017**, *10*, 1384–1399.

38. Fromstein, J.D.; Woodhouse, K.A. Elastomeric Biodegradable Polyurethane Blends for Soft Tissue Applications. Journal of Biomaterials Science Polymer Edition **2002**, *13*, 391–406.

39. Siemann, U. Solvent Cast Technology–a Versatile Tool for Thin Film Production, *In Scattering Methods and the Properties of Polymer Materials;* Springer: Berlin Heidelberg 2005; pp 1–14.

40. Ikada Y. *Tissue engineering: Fundamentals and Applications;* Vol. 8, Academic Press, 2011.

41. Basnett, P.; Ching, K.Y.; Stolz, M.; Knowles, J.C.; Boccaccini, A.R.; Smith, C.; Locke, I.C.; Keshavarz, T.; Roy, I. Novel Poly (3-hydroxyoctanoate)/Poly (3-hydroxybutyrate) Blends for Medical Applications. Reactive and Functional Polymers **2013**, *73*, 1340–1348.

42. Malandraki-Miller, S.; Tyser, R.; Riley, P.; Carr, C.A. Comparative Characterization of Cardiac Atrial Progenitor Cell Populations for Use in Cell Therapy. Heart **2014**, *100*, A14.

43. Srinivas M, Cruz LJ, Boneto F, Heerschap A, Figdor CG, de Vries IJM. Customizable, Multi-functional Fluorocarbon Nanoparticles for Quantitative In Vivo Imaging Using ^{19}F MRI and Optical Imaging. Biomaterials **2010**, *31*:7070–7077.

44. Constantinides, C.D.; Atalar, E.; McVeigh, E.R. Signal-to-noise Measurements in Magnitude Images from NMR Phased Arrays. Magnetic Resonance in Medicine **1997**, *38*, 852–857.

45. Ramalingam, S.; Vikram, M.; Vigneshbabu, M. P., Sivasankari, M. Flux Balance Analysis for Maximizing Polyhydroxyalkanoate Production in *Pseudomonas putida*. Indian Journal of Biotechnology **2011**, *10*, 70–74.

46. Lim, Y. C; Johnson J.; Fei, Z.; Wu, U.; Farson, D. F; Lannutti, J. J.; Choi, H. W., Lee, J. L. Micropatterning and Characterization of Electrospun Poly(ε-Caprolactone)/Gelatin Nanofiber Tissue Scaffolds by Femptosecond Laser Ablasion for Tissue Engineering Applications. Biotechnology and Bioengineering **2011**, *108,* 116–126.

47, Nanaki, S. G.; Pantopoulos, K.; Bikiaris, D. N. Synthesis of Biocompatible Poly(ε-caprolactone)-block-poly(propylene adipate) Copolymers Appropriate for Drug Nanoencapsulation in the Form of Core-shell Nanoparticles. International Journal of Nanomedicine **2011**, *6*, 2981–2995.

48. Constantinides, C.; Maguire, M.; Stork, L.; Swider, E.; Srinivas, M.; Carr, A.C.; Schneider, J.E. Temporal Accumulation and Localization of Isoflurane in the C57BL/6 Mouse and Assessment of its Potential Contamination in ^{19}F MRI with Perfluoro-crown Ether-labeled Cardiac Progenitor Cells at 9.4 T. Journal of Magnetic Resonance Imaging **2016**, DOI: 10.1002/jmri.25564.

49. Nomura, C.T.; Taguchi, S. PHA Synthase Engineering Toward Superbiocatalysts for Custom-made Biopolymers. Applied Microbiology and Biotechnology **2007**, *73*, 969–979.

50. Shishatskaya, E.I.; Volova, T.G.; Gitelson, I.I. In Vivo Toxicological Evaluation of Polyhydroxyalkanoates. Doklady Biological Sciences **2002**, *383*, 109–111.

51. Witholt, B. Kessler, B. Perspectives of Medium Chain Length Poly (hydroxyalkanoates), a Versatile Set of Bacterial Bioplastics. Current Opinion in Biotechnology **1999,** *10*, 279–285.

52. Stuckey, D.J.; Ishii, H.; Chen, Qi-Zhi; Boccaccini, A.R.; Hansen, U.; Carr, C.A.; Roether, J.A.; Jawad, H.; Tyler, D.J.; Ali, N.N.; Clarke, K.; Harding, S.E. Magnetic Resonance Imaging

Evaluation of Remodeling by Cardiac Elastomeric Tissue Scaffold Biomaterials in a Rat Model of Myocardial Infarction. Tissue Engineering: Part A **2010**, *16*, 3395–3402.

53. Eshraghi, S.; Das, S. Mechanical and Microstructural Properties of Polycaprolactone Scaffolds with One-dimensional, Two-dimensional, and Three-dimensional Orthogonally Oriented Porous Architectures Produced by Selective Laser Sintering. Acta Biomaterialia **2010**, *6*, 2467–2476.

54. Watanabe, S.; Shite, J., Takaoka, H.; Shinke, T.; Imuro, Y.; Ozawa, T.; Otake, H.; Matsumoto, D.; Ogasawara, D.; Peredes, O.; Yokoyama, M. Myocardial Stiffness is an Important Determinant of the Plasma Brain Natriuretic Peptide Concentration in Patients with both Diastolic and Systolic Heart Failure. European Heart J **2006**, *27*, 832–838.

55. Nagueh, S.; Shah, G.; Wu, Y.; Torre-Amione, G.; King, N.; Lahmers, S. Altered Titin Expression, Myocardial Stiffness and Left Ventricular Function in Patients with Dilated Cardiomyopathy. Circulation **2004**, *110*, 155–162.

56. Chen, Q.Z.; Bismarck, A.; Hansen, U.; Junaid, S.; Tran, M.Q.; Harding, S.W.; Ali, N.N.; Boccaccini, A.R. Characterisation of a Soft Elastomer Poly(glycerol sebacate) Designed to Match the Mechanical Properties of Myocardial Tissue. Biomaterials **2008**, *29*, 47–57.

57. Berry, M.F.; Engler, A.J.; Woo, Y.J.; Pirolli, T.J.; Bish, L.T.; Jayasankar, V.; Morine, K.J.; Gardner, T.J.; Discher, D.E.; Sweeney, H.L. Mesenchymal Stem Cell Injection after Myocardial Infarction Improves Myocardial Compliance. American Journal of Physiology Heart Circulatory Physiology **2006**, *290*, H2196–2203.

58. Reinecke, H.; Zhang, M.; Bartosek, T.; Murry, C.E. Survival, Integration, and Differentiation of Cardiomyocyte Grafts: a Study in Normalized Injured Rat Hearts. Circulation **1999**, *100*, 193–202.

59. Bursac, N. Cardiac Tissue Engineering using Stem Cells. IEEE Engineering in Medicine and Biology Magazine **2009**, *28*, 80–89.

60. Sofokleous, P.; Stride, E.; Bonfield, W; Edirisinghe, M. Design, Construction and Performance of a Portable Handheld Electrohydrodynamic Multi-needle Spray Gun for Biomedical Applications. Materials Science and Engineering: C **2013**, *33*, 213–223.

61. Lau, W. K.; Sofokleous, P.; Day, R; Stride, E; Edirisinghe, M. A Portable Device for In Situ Deposition of Bioproducts. Bioinspired, Biomimetic and Nanobiomaterials **2014**, *3*, 94–105.